EVS26
Los Angeles, California, May 6-9, 2012

Interaction between Self-Balanced Dicycle and Rider

Dein Shaw[1], Tzushin Hsieh 2[2]
[1]*Dein Shaw (Tzushin Hsieh) National Tsing Hua University, No. 101, Section 2, Kuang-Fu Road, Hsinchu, Taiwan 30013, R.O.C., dishaw@pme.nthu.edu.tw*

Abstract

Dicycle is a two-wheeled unicycle with two wheels axially aligned. The effect of interaction between a self-balanced dicycle and a rider has been investigated experimentally by measurements of state of motion. Dicycle can be seen as an inverted pendulum, which is an unstable system. The controller of the self-balanced dicycle and the rider control the balance of dicycle simultaneously. The controller controls the motor to afford torque, which keeps balance of the rider-dicycle system by moving dicycle forward and backward. At the same time, the state of stabilization changes when rider changes its posture or applies force on dicycle. The interaction between rider and controller can cause resonance of human-machine combined system. A method to investigate the resonance frequency under human operation is presented. The resonance frequency is estimated from a mathematical modal combining rider and inverted pendulum.

The dicycle is composed of seat, handlebars, and pedals installing on a Segway. The position of seat, handlebars, and pedals can be adjusted to suit different center of gravities of riders in order to keep controllability of Segway. Subjects rode under different conditions, which is riding forward and backward on level ground, crossing speed bump, and stopping abruptly after accelerating. The state of motion is measured through combined gyro sensor and accelerometer. A discussion of the design property of the self-balancing controller is made according to the reaction of riders.

Keywords: human-machine interaction, dynamic stabilization, personal transporter, self-balancing, human balance

1 Introduction

The examples of electrical personal assistive mobility device (EPAMD) with two-wheeled self-balancing ability are Segway (DEKA, 2001) and Winglet (Toyota, 2008). This kind of dicycle senses the inclinational state of itself and drives forward or backward to keep balancing, in other words, the position of center of mass of the rider controls the motion of the dicycle. The differences of rotational speed of the two coaxial wheels control the turning movement of the dicycle. A self-balanced dicycle, named i-Bike, is designed using the same controlling concept with additional pedals as shown in Figure 1. Unlike Segway and Winglet which is purely electric powered, i-Bike combines electrical and manual power. There are 3 operating modes: electrical mode, hybrid mode and manual mode. While operating under electrical mode, i-Bike is similar

to Segway and Winglet. Usually i-Bike is designed to operate under hybrid mode, which uses electric power for balancing and pedalling for driving. The power generated by pedalling can recharge the battery to better the efficiency. A prototype shown in Figure 1 base on the design concept of i-Bike is made in 2010[1].

Figure 1: i-Bike and the prototype

2 Interaction between the Dicycle and Rider

2.1 Research questions

The dynamic stability of the system is controlled by the controller and the rider simultaneously. According to previous researches, the factors of performance of balancing of the system can be identified as posture, biomechanics, interaction mode, center of mass (COM) of the system, controlling method, frequency response of the rider to the dicycle, and balancing ability of the rider.

The center of mass of the system is arranged according to the riding posture determined from human factors experiments. The electrical current of motor is controlled by balance controller according to the feedback signal of tilt angle, θ_v, and angular speed of tilting, $\dot{\theta}_v$. Constant values of parameters of controller respond to different inclination states are designed presently. The rotation speed of the wheels of dicycle has to be added into the control method in the future. The function of current of motor is shown as (1).

$$i = k_1\theta + k_2\theta^3 + k_3\dot{\theta} + k_4\dot{\phi} \qquad (1)$$

In above equation, i: current of motor, θ: tilt angle of dicycle and $\dot{\phi}$: rotation angle of wheel.

2.2 Assumptions

The condition discussed by this study is that the rider moves in the direction of forward and backward so the rider only interfere the controller with pitch motion. Under this circumstance, the rider and dicycle system is in a plane motion. The lateral force caused by the rider is balanced by two axial-aligning wheels which are assumed to be pure rolling on the ground. The dicycle and the rider are assumed to be rigid bodies when developing the equations of motion. The deformation and friction in between the components are neglected when finding the energy of the whole system.

The rider is simplified as a rotatable bar applying variable moment to the dicycle joints at the seat. The dicycle is simplified as an inverted pendulum with wheel rotating on the ground.

2.3 Mathematical model

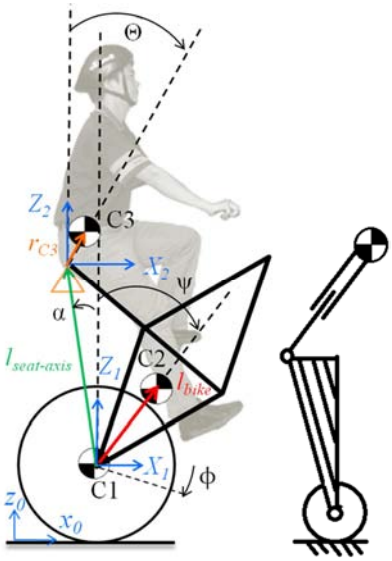

Figure 2: Mathematical model and simplified model

The rider and the dicycle are modeled as Figure 2 when riding. In Figure 2, three coordinate systems are set as follow: x_0z_0 is the contact point of wheels and ground at the beginning of motion, X_1Z_1 locates at the axle of wheels and shifts when the axle moves backward or forward, and X_2Z_2 sticks on the contact point of seat and rider and moves with the dicycle frame. The dicycle moves forward along the direction of x_0. The wheels rotate along Y_1 axis. C1, C2, and C3 locate the centre of mass of wheels, dicycle frame, and rider, respectively. Following are meanings of symbols in Figure 2:

L_{bike}: vector from axle to COM of dicycle frame.

$L_{seat\text{-}axle}$: vector from axle to seat.

L_{C3}: vector from sitting position to COM of rider.

α: initial angle between $L_{seat\text{-}axle}$ and z_0.
r: radius of wheel.
ϕ: rotation angle of wheel.
ψ: angle between Z_1 and L_{bike}.
Θ: angle between Z_2 and L_{C3}.

2.4 Equations of motion

Clockwise rotation denotes positive direction in the equations. Vectors are expressed in capital, like L_{bike}, $L_{seat\text{-}axle}$, and L_{C3}; Scalars are expressed in lowercase, like l_{bike}, $l_{seat\text{-}axle}$, and l_{C3}. Letter m and I represents mass and moment of inertia (MOI), respectively, and suffix 1, 2, and 3 represent wheels, dicycle frame, and rider, respectively.

2.4.1 Velocity and acceleration of COM of dicycle frame

The position of C2 is represented as R_{C2} respect to x_0z_0 coordinate. The Velocity and acceleration of C2 is represented as V_{C2} and A_{C2}, respectively. Vector $\hat{\imath}, \hat{\jmath}$ and $\hat{k}$ represent unit vector in the direction of x_0, y_0 and z_0, respectively. The absolute angular velocity of C2, $\dot{\psi}\,\hat{\jmath}$, is denoted as Ω_2.

$$\begin{aligned} R_{C2} &= R_{C1} + L_{bike} \\ &= \left(r\phi\hat{\imath} + r\hat{k}\right) + \left((\ell_{bike}\sin\psi)\hat{\imath} + (\ell_{bike}\cos\psi)\hat{k}\right) \end{aligned} \tag{2}$$

$$\begin{aligned} V_{C2} &= V_{C1} + V_{C2/C1} \\ &= r\dot{\phi}\hat{\imath} + \Omega_2 \times L_{bike} \\ &= r\dot{\phi}\hat{\imath} + \dot{\psi}\hat{\jmath} \times \left[(\ell_{bike}\sin\psi)\hat{\imath} + (\ell_{bike}\cos\psi)\hat{k}\right] \\ &= (r\dot{\phi} + \ell_{bike}\dot{\psi}\cos\psi)\hat{\imath} + (-\ell_{bike}\dot{\psi}\sin\psi)\hat{k} \end{aligned} \tag{3}$$

$$\begin{aligned} A_{C2} &= \frac{d}{dt}V_{C2} \\ &= r\ddot{\phi}\hat{\imath} + \dot{\Omega}_2 \times L_{bike} + \Omega_2 \times (\Omega_2 \times L_{bike}) \\ &= (r\ddot{\phi} + \ell_{bike}\ddot{\psi}\cos\psi - \ell_{bike}\dot{\psi}^2\sin\psi)\hat{\imath} \\ &\quad -(\ell_{bike}\ddot{\psi}\sin\psi + \ell_{bike}\dot{\psi}^2\cos\psi)\hat{k} \end{aligned} \tag{4}$$

2.4.2 Velocity and acceleration of COM of rider

The Position of C3 is represented as R_{C3}. The Velocity and acceleration of C3 is represented as V_{C3} and A_{C3}, respectively. The angle ψ between Z_1 and L_{bike} is summation of increment and its initial angle as shown in equation (5).

$$\psi = \psi_0 + \psi' \tag{5}$$

It is more convenient to use ψ' to describe the angle between L_{C3} and z_0 as summation of ψ' and Θ. The absolute angular velocity of C3, $(\dot{\psi} + \dot{\Theta})\hat{\jmath}$, is denoted as Ω_3.

$$\begin{aligned} R_{C3} &= R_{C1} + L_{seat-axis} + L_{C3} \\ &= r\phi\hat{\imath} + r\hat{k} \\ &\quad + (\ell_{seat-axis}\sin(\psi'-\alpha))\hat{\imath} + \ell_{seat-axis}\cos(\psi'-\alpha)\hat{k} \\ &\quad + (\ell_{C3}\sin(\psi'+\Theta))\hat{\imath} + \ell_{C3}\cos(\psi'+\Theta)\hat{k} \end{aligned} \tag{6}$$

$$\begin{aligned} V_{C3} &= V_{C1} + \Omega_2 \times L_{seat-axis} + \left((\dot{L}_{C3})_{x_2z_2} + \Omega_3 \times L_{C3}\right) \\ &= r\dot{\phi}\hat{\imath} \\ &\quad + \begin{pmatrix} (\dot{\ell}_{C3})_{x_2z_2}\sin(\Theta+\psi') + \ell_{C3}(\dot{\Theta}+\dot{\psi})\cos(\Theta+\psi') \\ + \ell_{seat-axis}\dot{\psi}\cos(\psi'-\alpha) \end{pmatrix}\hat{\imath} \\ &\quad + \begin{pmatrix} (\dot{\ell}_{C3})_{x_2z_2}\cos(\Theta+\psi') - \ell_{C3}(\dot{\Theta}+\dot{\psi})\sin(\Theta+\psi') \\ - \ell_{seat-axis}\dot{\psi}\sin(\psi'-\alpha) \end{pmatrix}\hat{k} \end{aligned} \tag{7}$$

The expression $(\dot{L}_{C3})_{x_2z_2}$ in equation (7) denotes the radial component of velocity in the coordinate system X_2Z_2 (i.e., the stretching speed of l_{C3}).

$$\frac{d}{dt}(L_{C3})_{x_2z_2} = (\ddot{L}_{C3})_{x_2z_2} + (\dot{\Theta}\,\hat{\jmath}) \times (\dot{L}_{C3})_{x_2z_2} \tag{8}$$

$$\begin{aligned} A_{C3} &= \frac{d}{dt}V_{C3} \\ &= A_{C1} + \dot{\Omega}_2 \times L_{seat-axis} + \Omega_2 \times \frac{d}{dt}(L_{seat-axis}) \\ &\quad + \frac{d}{dt}\left[(\dot{L}_{C3})_{x_2z_2}\right] + \dot{\Omega}_3 \times L_{C3} + \Omega_3 \times \frac{d}{dt}(L_{C3}) \\ &= A_{C1} + \dot{\Omega}_2 \times L_{seat-axis} + \Omega_2 \times (\Omega_2 \times L_{seat-axis}) \\ &\quad + \left[(\ddot{L}_{C3})_{x_2z_2} + (\dot{\Theta}\,\hat{\jmath}) \times (\dot{L}_{C3})_{x_2z_2}\right] + \dot{\Omega}_3 \times L_{C3} \\ &\quad + \Omega_3 \times \left[(\dot{L}_{C3})_{x_2z_2} + \Omega_3 \times L_{C3}\right] \end{aligned} \tag{9}$$

$$\begin{aligned} &= A_{C1} + (\Omega_2 \times \Omega_2) \times L_{seat-axis} + \dot{\Omega}_2 \times L_{seat-axis} \\ &\quad + (\ddot{L}_{C3})_{x_2z_2} + (\dot{\Theta}\,\hat{\jmath} + \Omega_3) \times (\dot{L}_{C3})_{x_2z_2} \\ &\quad + \Omega_3 \times \Omega_3 \times L_{C3} + \dot{\Omega}_3 \times L_{C3} \end{aligned}$$

2.4.3 Equation of motion

The kinetic and potential energy of rider-dicycle system is shown below.

$$\begin{aligned} T &= \frac{1}{2}m_1\dot{x}^2 + \frac{1}{2}I_1\dot{\phi}^2 + \frac{1}{2}m_2V_{C2}^2 + \frac{1}{2}I_2\dot{\psi}^2 \\ &\quad + \frac{1}{2}m_3V_{C3}^2 + \frac{1}{2}I_3(\dot{\Theta}+\dot{\psi})^2 \end{aligned} \tag{10}$$

$$\begin{aligned} V &= m_2 g\ell_{bike}\cos\psi \\ &\quad + m_3 g\left[\ell_{C3}\cos(\Theta+\psi') + \ell_{seat-axis}\cos(\alpha-\psi')\right] \end{aligned} \tag{11}$$

$$\begin{aligned} L &= T - V \\ &= \frac{1}{2}m_1\dot{x}^2 + \frac{1}{2}I_1\dot{\phi}^2 + \frac{1}{2}m_2V_{C2}^2 + \frac{1}{2}I_2\dot{\psi}^2 \\ &\quad + \frac{1}{2}m_3V_{C3}^2 + \frac{1}{2}I_3(\dot{\Theta}+\dot{\psi})^2 \end{aligned} \tag{12}$$

$$-\left\{\begin{matrix} m_2 g \ell_{bike} \cos\psi \\ +m_3 g\left[\begin{matrix} \ell_{C3}\cos(\Theta+\psi') \\ +\ell_{seat-axis}\cos(\alpha-\psi') \end{matrix}\right] \end{matrix}\right\}$$

The Euler-Largrange equation :

$$\begin{cases} \dfrac{d}{dt}\left(\dfrac{\partial L}{\partial \dot{\phi}}\right)-\dfrac{\partial L}{\partial \phi}=\tau_{wheel} \\ \dfrac{d}{dt}\left(\dfrac{\partial L}{\partial \dot{\psi}}\right)-\dfrac{\partial L}{\partial \psi}=-\tau_{wheel}-\tau_{human} \\ \dfrac{d}{dt}\left(\dfrac{\partial L}{\partial \dot{\Theta}}\right)-\dfrac{\partial L}{\partial \Theta}=\tau_{human} \end{cases} \quad (13)$$

The equations of motion are derived by submitting Eqs 10-12 into Eq. 13 and are listed as following:

$$\begin{aligned} &(m_1+m_2+m_3)r^2\ddot{\phi}+I_1\ddot{\phi} \\ &+m_2 r\ell_{bike}\left(\ddot{\psi}\cos\psi-\dot{\psi}^2\sin\psi\right) \\ &+m_3 r\left[\left(\ddot{\ell}_{C3}\right)_{x2z2}\sin(\Theta+\psi')\right. \\ &\quad +2\left(\dot{\ell}_{C3}\right)_{x2z2}\left(\dot{\Theta}+\dot{\psi}\right)\cos(\Theta+\psi') \\ &\quad +\ell_{C3}(\ddot{\Theta}+\ddot{\psi})\cos(\Theta+\psi') \\ &\quad -\ell_{C3}\left(\dot{\Theta}+\dot{\psi}\right)^2\sin(\Theta+\psi') \\ &\quad -\ell_{C3}\left(\dot{\Theta}+\dot{\psi}\right)^2\sin(\Theta+\psi') \\ &\quad +\ell_{seat-axis}\ddot{\psi}\cos(\psi'-\alpha) \\ &\quad \left.-\ell_{seat-axis}\dot{\psi}^2\sin(\psi'-\alpha)\right] \\ &=\tau_{wheel} \end{aligned} \quad (14)$$

$$\begin{aligned} &m_2\ell_{bike}{}^2\ddot{\psi}+m_2 r\ell_{bike}\ddot{\phi}\cos\psi+I_2\ddot{\psi} \\ &+m_3\left(\ddot{\Theta}+\ddot{\psi}\right)\ell_{C3}^2+2m_3\ell_{C3}\left(\dot{\ell}_{C3}\right)_{x2z2}\left(\dot{\Theta}+\dot{\psi}\right) \\ &+m_3\ell_{seat-axis}{}^2\ddot{\psi}+m_3 r\ell_{C3}\ddot{\phi}\cos(\Theta+\psi') \\ &+m_3 r\ell_{seat-axis}\ddot{\phi}\cos(\psi'-\alpha) \\ &+m_3\ell_{seat-axis}\left(\ddot{\ell}_{C3}\right)_{x2z2}\sin(\Theta+\alpha) \\ &+2m_3\ell_{seat-axis}\left(\dot{\ell}_{C3}\right)_{x2z2}\left(\dot{\Theta}+\dot{\psi}\right)\cos(\Theta+\alpha) \\ &+m_3\ell_{C3}\ell_{seat-axis}\left[\begin{matrix}\left(\ddot{\Theta}+2\ddot{\psi}\right)\cos(\Theta+\alpha) \\ -\left(\dot{\Theta}+2\dot{\psi}\right)\dot{\theta}\sin(\Theta+\alpha)\end{matrix}\right] \\ &+I_3\left(\ddot{\Theta}+\ddot{\psi}\right)-m_2 g\ell_{bike}\sin\psi \\ &-m_3 g\ell_{C3}\sin(\Theta+\psi') \\ &+m_3 g\ell_{seat-axis}\sin(\alpha-\psi') \\ &=-\tau_{wheel}-\tau_{human} \end{aligned} \quad (15)$$

$$\begin{aligned} &m_3\ell_{C3}^2\left(\ddot{\Theta}+\ddot{\psi}\right)+2m_3\ell_{C3}\left(\dot{\ell}_{C3}\right)_{x2z2}\left(\dot{\Theta}+\dot{\psi}\right) \\ &+m_3 r\ell_{C3}\ddot{\phi}\cos(\Theta+\psi') \\ &+m_3\ell_{C3}\ell_{seat-axis}\ddot{\psi}\cos(\Theta+\alpha)+I_3\left(\ddot{\Theta}+\ddot{\psi}\right) \\ &+m_3\ell_{C3}\ell_{seat-axis}\dot{\psi}^2\sin(\Theta+\alpha) \\ &-m_3 g\ell_{C3}\sin(\Theta+\psi') \\ &=\tau_{human} \end{aligned} \quad (16)$$

2.5 Resonance of the system

2.5.1 Simplified model

It is found that Eqs. 14-16 are nonlinear equations and it is hard to find the resonance frequencies. Therefore, a simplified model shown in Figure 3 is used. Rider and dicycle frame are taken as one body which COM controls the rotation speed of wheels and two wheels are taken as another body. Mass and MOI of the inverted pendulum (which is composed of rider and dicycle frame) are expressed as m_p and I_p, respectively. Mass and MOI of the wheel body are expressed as m_w and I_w, respectively. After simplification, Eqs. 14-16 can be simplified. The derived equations of motion of the simplified model are expressed as equation (17) and (18).

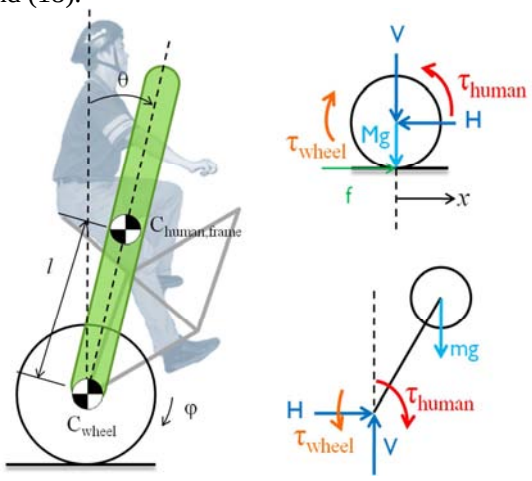

Figure 3: Simplified model and free-body diagram

$$\begin{aligned} (\tau_{wheel}-\tau_{human}) &= (I_{wheel}+m_w r^2+m_p r^2)\ddot{\phi} \\ &\quad -m_p rl\dot{\theta}^2\sin\theta+m_p rl\ddot{\theta}\cos\theta \end{aligned} \quad (17)$$

$$\begin{aligned} (\tau_{wheel}-\tau_{human}) &= (-m_p rl\cos\theta)\ddot{\phi}-(I_p+m_p l^2)\ddot{\theta} \\ &\quad +m_p gl\sin\theta \end{aligned} \quad (18)$$

In above equations, where *l*: distance of COM of inverted pendulum to axle. *r*: radius of wheels. θ: tilt angle of the pendulum. ϕ: rotation angle of wheels.

Relation between torque inputs and angle outputs is shown in equation (19) by rearranging equation (17) and (18).

$$\begin{aligned}
&\Delta\times\ddot{\phi}+\left[\left(I_p+m_pl^2\right)m_prl\dot{\theta}\sin\theta\right]\dot{\theta}\\
&-m_pgl\cdot m_prl\cos\theta\cdot\theta\\
&\quad=-\left(I_p+m_pl^2+m_prl\cos\theta\right)\left(\tau_{wheel}-\tau_{human}\right)\\
&\Delta\times\ddot{\theta}-\left[\left(m_prl\right)^2\sin\theta\cos\theta\cdot\dot{\theta}\right]\dot{\theta}\\
&+m_pgl\left(I_w+m_wr^2+m_pr^2\right)\theta\\
&\quad=\begin{pmatrix}m_prl\cos\theta\\+I_w+m_wr^2+m_pr^2\end{pmatrix}\left(\tau_{wheel}-\tau_{human}\right)\\
&\Delta=\det\left(\begin{bmatrix}I_w+m_wr^2+m_pr^2 & m_prl\cos\theta\\ -m_prl\cos\theta & -I_p-m_pl^2\end{bmatrix}\right)\\
&\quad=\det\begin{bmatrix}a_{11} & a_{12}\\ a_{21} & a_{22}\end{bmatrix}=\det(A)
\end{aligned}\tag{19}$$

The torque of wheel, τ_{wheel}, which is drove by brushless DC motor, is proportional to current of motor shown in equation (1).

$$\begin{aligned}
\tau_{wheel}&=ki\\
&=k\left(k_1\theta+kk_2\theta^3+kk_3\dot{\theta}+kk_4\dot{\phi}\right)\\
&=k_1'\theta+k_2'\theta^3+k_3'\dot{\theta}+k_4'\dot{\phi}
\end{aligned}\tag{20}$$

The motion of equation is rearranged by substituting equation (20) for torque of wheel. The parameter k_4' is zero because the feedback signal of rotation speed has not been included in present balance controlling. Finally, the equations can be expressed as:

$$\begin{aligned}
&\Delta\times\ddot{\phi}+k_4'\left(m_prl\cos\theta+I_p+m_pl^2\right)\dot{\phi}\\
&+\left[\left(I_p+m_pl^2\right)\left(m_prl\dot{\theta}\sin\theta+k_3'\right)+k_3'm_prl\cos\theta\right]\dot{\theta}\\
&-m_pgl\cdot m_prl\cos\theta\cdot\sin\theta\\
&=-\left(I_p+m_pl^2+m_prl\cos\theta\right)\left(k_1'\theta+k_2'\theta^3-\tau_{human}\right)
\end{aligned}\tag{21}$$

$$\begin{aligned}
&\Delta\times\ddot{\theta}-k_4'\left(m_prl\cos\theta+I_w+m_wr^2+m_pr^2\right)\dot{\phi}\\
&-\begin{bmatrix}k_3'\left(m_prl\cos\theta+I_w+m_wr^2+m_pr^2\right)\\+\left(m_prl\right)^2\sin\theta\cos\theta\cdot\dot{\theta}\end{bmatrix}\dot{\theta}\\
&-\left(m_prl\cos\theta+I_w+m_wr^2+m_pr^2\right)\left(k_1'\theta+k_2'\theta^3\right)\\
&+m_pgl\left(I_w+m_wr^2+m_pr^2\right)\sin\theta\\
&=-\left(m_prl\cos\theta+I_w+m_wr^2+m_pr^2\right)\tau_{human}
\end{aligned}\tag{22}$$

2.5.2 Resonance of the system

Linearization of equation of motion at θ which is close to zero is shown in equation (23) to discuss condition and frequency of resonance of the rider-dicycle system.

Equation of Motion Linearization at $\theta=0$

$$\sin\theta\approx\sin(0)+\left.\frac{d\sin\theta}{d\theta}\right|_{\theta=0}\cdot(\theta-0)=\theta$$

$$\cos\theta\approx\cos(0)+\left.\frac{d\cos\theta}{d\theta}\right|_{\theta=0}(\theta-0)=1$$

Let $\dot{\theta}_0$ *be the initial angular speed*,

$$\begin{aligned}
\sin\theta\cdot\dot{\theta}^2&\approx\sin(0)\cdot\dot{\theta}_0^2+\left.\frac{\partial\left(\sin\theta\cdot\dot{\theta}^2\right)}{\partial\theta}\right|_{\substack{\theta=0\\\dot{\theta}=\dot{\theta}_0}}\cdot(\theta-0)\\
&\quad+\left.\frac{\partial\left(\sin\theta\cdot\dot{\theta}^2\right)}{\partial\dot{\theta}}\right|_{\substack{\theta=0\\\dot{\theta}=\dot{\theta}_0}}\cdot(\dot{\theta}-\dot{\theta}_0)\\
&=\theta\dot{\theta}_0^2
\end{aligned}$$

$$\begin{aligned}
\cos\theta\cdot\dot{\theta}&\approx\cos(0)\cdot\dot{\theta}_0+\left.\frac{\partial\left(\cos\theta\cdot\dot{\theta}\right)}{\partial\theta}\right|_{\substack{\theta=0\\\dot{\theta}=\dot{\theta}_0}}\cdot(\theta-0)\\
&\quad+\left.\frac{\partial\left(\cos\theta\cdot\dot{\theta}\right)}{\partial\dot{\theta}}\right|_{\substack{\theta=0\\\dot{\theta}=\dot{\theta}_0}}\cdot(\dot{\theta}-\dot{\theta}_0)\\
&=\dot{\theta}
\end{aligned}\tag{23}$$

The linearized equations of motion are shown as below.

$$\begin{aligned}
&\det(A)\cdot\ddot{\phi}+k_3'\left(I_p+m_pl^2+m_prl\right)\dot{\theta}\\
&+\left(I_p+m_pl^2+m_prl\cos\theta\right)\cdot k_1'\theta\\
&=\left(I_p+m_pl^2+m_prl\cos\theta\right)\tau_{human}
\end{aligned}\tag{24}$$

$$\begin{aligned}
&\det(A)\cdot\ddot{\theta}-k_3'\left(m_prl+I_w+m_wr^2+m_pr^2\right)\dot{\theta}\\
&+\begin{bmatrix}m_pgl\left(I_w+m_wr^2+m_pr^2\right)-\left(m_prl\right)^2\dot{\theta}_0^2\\-k_1'\left(m_prl+I_w+m_wr^2+m_pr^2\right)\end{bmatrix}\theta\\
&=-\left(m_prl+I_w+m_wr^2+m_pr^2\right)\tau_{human}
\end{aligned}\tag{25}$$

When the system is balanced and the tilt angle is very small, the relation between torque inputs and output, which is the tilt angle, θ, of the pendulum, is shown in equation (25).

When the initial inclinational speed, $\dot{\theta}_0$, satisfies the condition shown in equation (26) and (27), the resonant frequency is expressed in equation(28).

$$m_p gl\left(I_w + m_w r^2 + m_p r^2\right)$$

$$< \left(m_p rl\right)^2 \dot{\theta}_0{}^2 + k_1' \begin{pmatrix} m_p rl \\ + I_w + m_w r^2 + m_p r^2 \end{pmatrix} \quad (26)$$

$$\dot{\theta}_0 > \left(\begin{array}{l} \dfrac{g\left(I_w + m_w r^2 + m_p r^2\right)}{m_p r^2 l} \\ - \dfrac{k_1'\left(m_p rl + I_w + m_w r^2 + m_p r^2\right)}{\left(m_p rl\right)^2} \end{array} \right)^{\frac{1}{2}}$$

damping ratio $\zeta =$

$$\frac{k_3'\left(m_p rl + a_{11}\right)}{2 \times \sqrt{-\det(A) \cdot \begin{pmatrix} k_1'\left(m_p rl + a_{11}\right) \\ + \left(m_p rl\right)^2 \dot{\theta}_0{}^2 - m_p gla_{11} \end{pmatrix}}} \quad (27)$$

$$< \frac{1}{\sqrt{2}}$$

resonant frequency

$$f_r = \frac{\omega_r}{2\pi}$$

$$= \frac{1}{2\pi} \omega_0 \sqrt{1 - 2\zeta^2}$$

$$f_r{}^2 = \frac{1}{4\pi^2\left(-\det(A)\right)} \begin{bmatrix} k_1'(a_{11} + a_{12}) + a_{12}{}^2 \dot{\theta}_0{}^2 \\ - m_p gla_{11} \\ + \dfrac{k_3'^2 (a_{11} + a_{12})^2}{2\det(A)} \end{bmatrix} \quad (28)$$

$$\omega_0 = \sqrt{\frac{m_p gl\left(I_w + m_w r^2 + m_p r^2\right) - \left(m_p rl\right)^2 \dot{\theta}_0^2 - k_1'\left(m_p rl + I_w + m_w r^2 + m_p r^2\right)}{\det(A)}}$$

When the tilt angle, θ, is very small, the condition that causes the rider-dicycle system to resonate is related to angular velocity of the pendulum; that is, when the angular velocity of the pendulum exceeds a specific limit, and the frequency of the torque applied by rider equals the resonant frequency, the maximum of tilt angle is reached under interaction of the rider and the controller.

The specific limit of angular velocity of the pendulum for the system to resonate is lowered when the feedback value k_1 is increased, in other words, the greater value of k_1 is, the more the system tends to lose control. The limit of angular velocity is related only to MOI of wheels, not of the rider or the dicycle frame. And the lower the position of COM of the system is, the more stable it is.

The parameters, k_1' and k_3' in the expression of torque of wheel (equation (20)), must satisfy the following conditions which are deduced from equation (26) and (27) to avoid resonance of the rider-dicycle system.

$$k_1' \le \frac{m_p gl\left(I_w + m_w r^2 + m_p r^2\right) - \left(m_p rl\right)^2 \dot{\theta}_0{}^2}{\left(m_p rl + I_w + m_w r^2 + m_p r^2\right)} \quad (29)$$

The rider-dicycle system remains stable if the value of k_1' is in a specific range. If k_1' has exceeded the range, then k_3' has to be greater than what expressed in equation **錯誤! 找不到參照來源。** to stabilize the system by way of making the system an under damping system.

$$k_3' \ge \frac{\sqrt{2} \times \sqrt{-\det(A) \cdot \begin{pmatrix} k_1'\left(m_p rl + a_{11}\right) \\ + \left(m_p rl\right)^2 \dot{\theta}_0{}^2 - m_p gla_{11} \end{pmatrix}}}{\left(m_p rl + a_{11}\right)} \quad (30)$$

3 Experiment of Interaction between Rider and Dicycle

3.1 Objective

The aim of the experiment is to observe the reaction of rider and dicycle under specially unbalance circumstance that the rider-dicycle system keeps moving along anterior-posterior direction. The movement of the system combining rider with dicycle is interfered by both human and the balancing controller which has not been ready for normal driving operation. A test bed therefore is built in this study to simulate the action of functional balancing controller in order to measure the state of motion of the rider-dicycle system. The result of experiment may be reference for the design of controller.

3.2 Apparatus

In this study, a Segway combines with frame structure to simulate the self-balancing dicycle due to the principles of control are same. The frame structure is designed to satisfy the human factor data and is adjustable for different rider.

3.2.1 Main structure

The apparatus for simulating the real self-balancing dycycle was made according to the evaluation of acceleration and space needs during operation. The adjustable frame installed on Segway is able to let the rider and the dicycle keep

balance and still, and was designed to follow the operating rules of Segway.

The original operation process of Segway is that the inclination of the dicycle must be within the limit to start the power up, that one of four pressure sensors under the mat must be pressed to start and keep the balancing function, that the power is unable to be turned off when the pressure sensor was pressed, and that the motor applies an extra torque to lessen the tilt angle of the dicycle when exceeding the default speed limit.

Both Segway and the design of dicycle frame, which is based on i-Bike as well as the result of study of comfortableness, are modelled and assembled with Solidworks to evaluate MOI and the position of COM in order to calculate the state of motion and load of the frame.

The main structure of dicycle frame is shown in Figure 4. The seat is able to slide on the aluminum frame, MISUMI HFSH8-4040, to adjust its position. The pedals which assembled with aluminium frame, MISUMI HFS5-2040, are installed on the control shaft as shown in Figure 5.

The dimension and position of pedals, handlebar, and seat of the original design of i-Bike, prototype and the test frame in this study is indicated (in millimeter) in Figure 6.

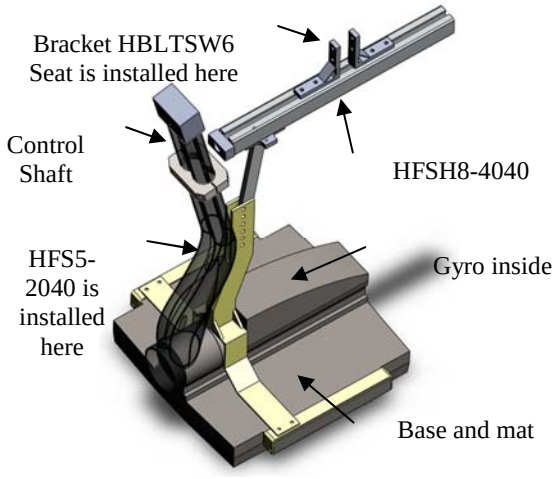

Figure 4: The main structure of test frame

Figure 5: Adjustability range

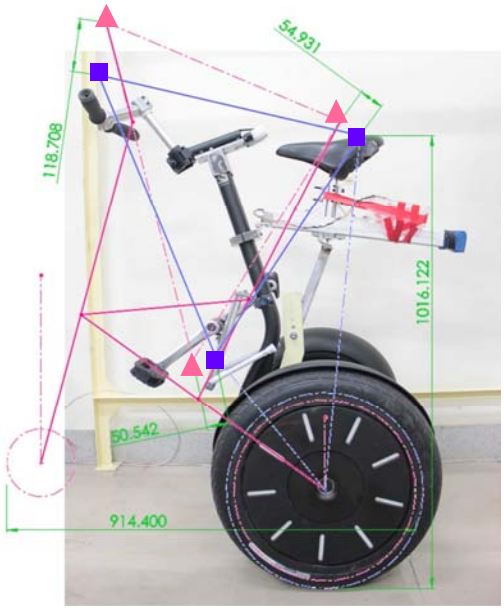

Figure 6: i-Bike(▲), prototype(■), and test frame

3.2.2 Safety device

There are safety devices, including helmet and harness which connects with the rope above the test route, to ensure subjects against falling when the dicycle is unbalanced.

Table 1

Subjects	A	B	C	D	E	F	G	mean	S.D.
Stature (cm)	178	177	181	181	172	167.5	166	174.64	6.20
Weight (kg)	67	70	71	70	67	62.1	57.5	66.37	4.92
l_{C3} (cm)	33.1	32.9	33.7	33.7	32.0	31.2	30.9	32.49	1.15
MOI about y-axis (kg·m^2)	8.21	8.33	8.86	8.78	7.54	6.65	6.13	7.786	1.057
MOI about sitting point	15.56	15.92	16.91	16.72	14.40	12.69	11.61	14.830	2.031

Figure 7: Safety devices and the test bed

Each end of the static rope is tie to iron rack via a carabiner, and the pulley on the rope allows the harness to move along x-axis shown in Figure 7. The iron rack is 2.5 meters long, 1.2 meters wide and 2 meters high. A 3 meters long and 1 meter wide slip-proof mat is used to prevent skidding.

3.2.3 Measuring method

An ADXL335 accelerometer and a LISY300AL gyroscope were combined in this study to measure the state of motion. The tilt, angular velocity, and angular acceleration can be measured simultaneously via sensor fusion.
The tilt angle is derived by means of combining low-frequency signal from the accelerometer and high-frequency signal from the gyroscope.

3.3 Experiments

3.3.1 Assumptions

The reference for measuring the distance between the pedal, seat, and the handlebar is the geometrical center of each part. Variables that height and weight of different subjects were considered in this study and the differences in age, energy, physical coordination were neglected. The position of COM of each subject was estimated from statistical data.
The changing position of COM of subjects was neglected when the subjects moved their limbs, so the position of COM of subjects was assumed rotating about the contact point on the seat, and the rotating radius was assumed constant, that is, $\left(\dot{L}_{C3}\right)_{x_2z_2}$ and $\left(\ddot{L}_{C3}\right)_{x_2z_2}$ in equation (8) and (9) are zero.

3.3.2 Procedure

At the beginning of each test, weights had to be put on the mat before the subjects got on the dicycle to keep the balancing controller functioning. Two ground conditions were investigated in this study; one was flat, slip-proofed and the other was with a 5-cm-high speed bump. The subjects were asked to drive the dicycle three times under each of the five conditions, which were driving forward on flat ground, driving backward on flat ground, passing forward a speed bump, passing backward a speed bump, and stop suddenly on flat ground. The sensors recording the state of motion of the system were placed on the dicycle frame and on waistband of the harness.

3.3.3 Subjects

The weights and statures of seven subjects aged 20 to 30 are listed in Table 1. MOI and the position of COM of subjects are evaluated by national anthropometric database of worker population and the regression functions derived by Santschi, et al.

3.4 Results

The tilt angle, angular speed, and angular acceleration was recorded when the subjects drove the dicycle forward and backward, and stop suddenly on flat and speed-bumped ground.
The ranges of tilt angle of subjects and dicycle under different circumstances are shown in Figure 8.

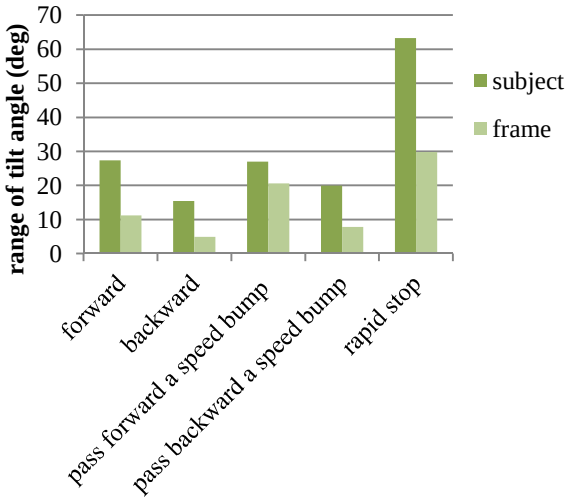

Figure 8: Range of tilt angle of subject and frame

3.4.1 Correlation of swing frequency and properties of controlling parameters

To avoid resonance of the rider-dicycle system, the condition of controlling parameters, k_1' and k_3', can be derived by substituting the tilting velocity measured for $\dot{\theta}_0$ in equation (29) and (30). The swing frequency is assumed to be the resonance frequency of the rider-dicycle system when the dicycle swinging intensely, and the relation of parameter k_1' and k_3' can be derived from equation (28).

Experiment results in which the largest and second largest tilt angle occurred were analysed, which are under the condition of passing forward a speed bump and rapid stop. The orthogonal frequency spectrum of tilt angle, angular velocity, angular acceleration, and driving acceleration of the subjects are shown in Figure 9 and Figure 10. The swinging frequency of the dicycle is from 1.076 Hz to 1.174 Hz when the dicycle was passing forward a speed bump; and the frequency is 0.881 Hz when the dicycle stop rapidly.

The angular velocity at the tilt angle of the dicycle and the subjects were zero was found to determine the properties of k_1' and k_3' using equation (29) and (30).

After deriving the ranges of the parameters, the different range of parameters such as position of COM and MOI of the subjects were discussed. The variables tested are normal distribution.

The range of k_1' is increased with higher position of COM and greater MOI as shown in Figure 11. Contrarily, change of k_3' corresponding to COM and MOI is unclear. The correlation of parameters and the inclinational angular speed are shown in Figure 14.

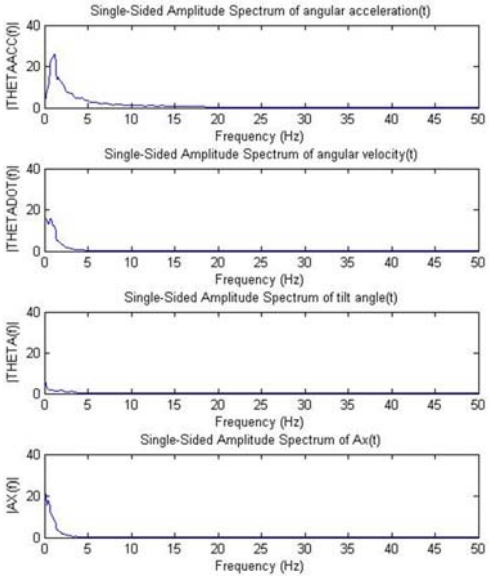

Figure 9: Frequency spectrum of state of motion when dicycle passing forward a speed bump

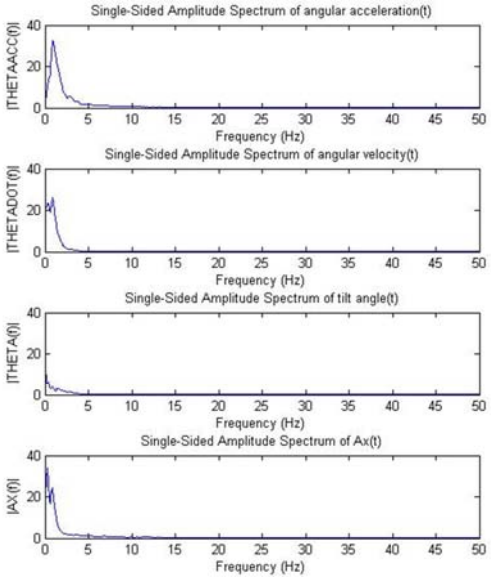

Figure 10: Frequency spectrum of state of motion when dicycle stopping rapidly

3.4.2 Correlation of subjects and state of motion

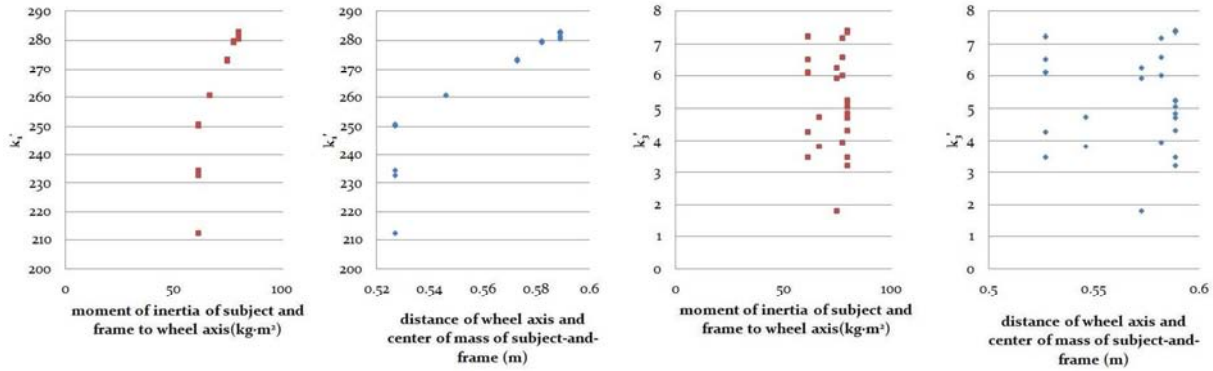

Figure 11: Parameters corresponding to different COM and MOI

For each subjects, the spectrums of state of motion from three results under the same condition were compared. The swing frequencies shows similarity and driving skill has no significant effect on swing frequency.

The response of subjects of different positions of COM and MOI are shown in Figure 12 and Figure 13. The response shows little correlation with COM and MOI of subjects, and the largest response occurred when the subjects stops rapidly.

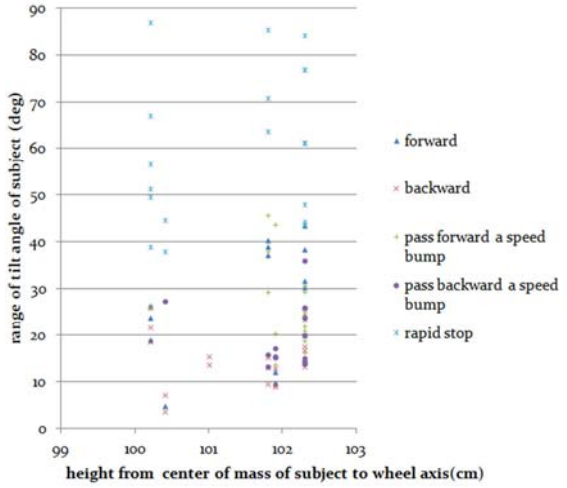

Figure 12: Corresponding response of position of COM of subjects

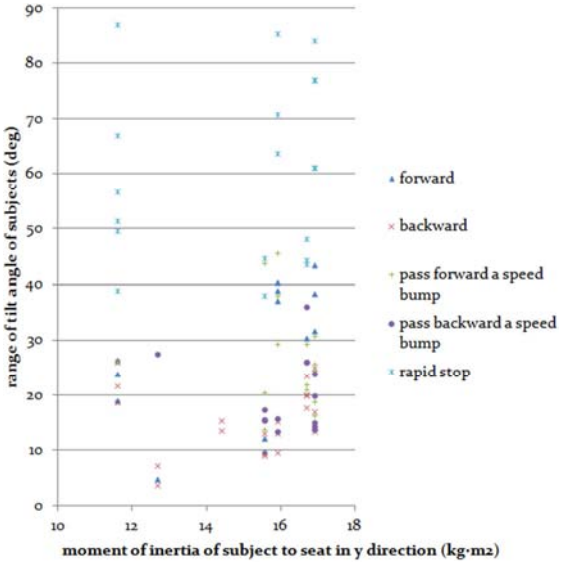

Figure 13: Corresponding response of MOI of subjects

4 Conclusion

The results of experiment were summarized and some considerations for control strategy as well as feedbacks from subjects are proposed in this study. The mathematical model combining rider and self-balancing dicycle is provided in this study for deriving the properties of the system when designing the balancing controller. The mode of interaction with riders and performance of dicycle

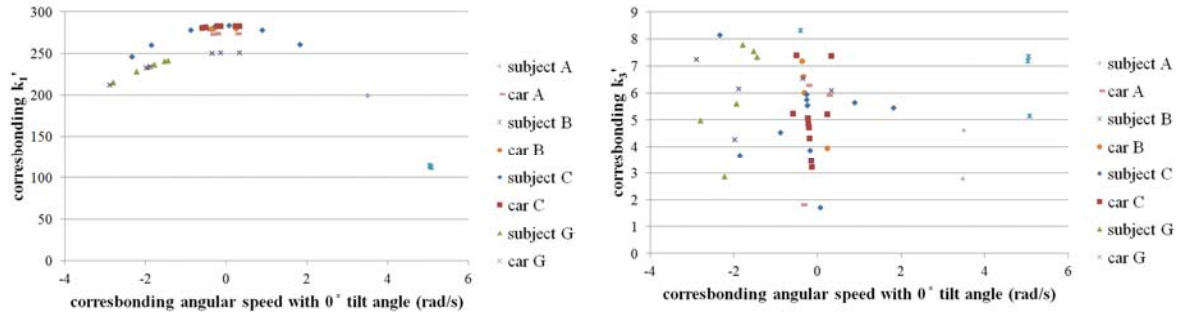

Figure 14: Parameters corresponding to different inclinational angular speed

is able to be observed by the apparatus to improve the usability of the dicycle.

4.1 Interaction between dicycle and rider

In some cases, riders fell from the Segway because they stop rapidly or inclined on the Segway suddenly which overloaded the motor. Another reason for falling is that during the motion of swinging, the feet of the riders leave the mat so the controller of Segway turns off its power of balancing. Compare Segway to the dicycle in this study, the situation of losing control has rarely been observed from the results of experiments because of the following reasons.
First, it is difficult for the subjects to actively make the dicycle lose control. Secondly, a sitting posture limits the moving range of position of COM and makes the rider-dicycle system more stable. Finally, the space for the subjects to accelerate the dicycle was 3 meters long, which might not be sufficient for the dicycle to achieve a high speed. A wireless data acquisition device is suggested for a long accelerative distance.
Braking mechanism has to be design in the future because that controlling the position of COM in order to stop the dicycle was difficult and uncomfortable for the riders in a sitting posture comparing to the riders in a standing posture when driving a Segway. The design of braking mechanism must consider the interacting mode of rider and dicycle to avoid toppling the rider. The speed limit and properties of the rider-dicycle system corresponding to different design of controller can be derived from the mathematical model. And the pedal mechanism is more appropriate for the riders to control the dicycle.

4.2 Usability

The dicycle frame of the test bed in this study was designed to drive straight, but the structure is liable to cause unsymmetrical loads and make the dicycle turns. To avoid turning, the seat may not be assembled with the control shaft.
As to the seat, the position is too high for most of subjects, and sitting on it is not comfortable for the subjects to move continuously. The pedals are idling when the dicycle was in electrical mode, so it is more comfortable for the riders if they are able to step on a footrest as a support for balancing.

References

[1] Y.L. Chang, *Transmission Design of a Self Balanced Double-Wheel Unicycle*, in Master thesis, PME. Dept. 2010, NTHU: Hsinchu. p. 62.

[2] K. Boniface et al., *Serious Injuries Related to the Segway® Personal Transporter: A Case Series*. Annals of Emergency Medicine, ISSN 0196-0644, 57(4) (2011), 370-374.

[3] Peterka et al., *Sensorimotor Integration in Human Postural Control.* J Neurophysiol, ISSN 0022-3077, 88(2002), 1097-1118.

[4] NeuroCom® International, I., EquiTest, in NeuroCom Balance Manager Systems & Products, Natus®, Editor. 2004: USA.

[5] J.Y. Lee, *Design and Development of a 3-DOF Balance System*, in BME Dept. 2003, NCKU: Tainan. p. 78.

[6] Formal'skii et al., *An inverted pendulum on a fixed and a moving base*. Journal of Applied Mathematics and Mechanics, ISSN 0021-8928, 70(1) (2006), 56-64.

[7] Graichen et al., *Swing-up of the double pendulum on a cart by feedforward and feedback control with experimental validation*. Automatica, ISSN 0005-1098, 43(1) (2007), 63-71.

[8] Wilczynski et al., *Dynamic system model for estimating surface-induced frame loads during off-road cycling*. Journal of Mechanical Design, Transactions of the ASME, ISSN 1050-0472, 116(1994), 816-822

[9] Wang, E.L. et al., *A dynamic system model of an off-road cyclist.* Transactions of the ASME. Journal of Biomechanical Engineering, ISSN 0148-0731, 119(1997)(Copyright 1997, IEE), 248-53

[10] Waechter et al., *A multibody model for the simulation of bicycle suspension systems.* Dicycle System Dynamics, ISSN 0042-3114, 37(2002) (Copyright 2002, IEE), 3-28

[11] Qichang et al., *Full bicycle dynamic model for interactive bicycle simulator.* Transactions of the ASME. Journal of Computing and Information Science in Engineering, ISSN 1746-7659, 5(2005) (Copyright 2005, IEE), 373-80.

[12] Santschi et al., *Moments of inertia and centers of gravity of the living human body.* 1963, Aerospace Medical Research Laboratory document AMRL TDR-63-36: Ohio.

[13] J. K. Moore et al., *A Method for Estimating Physical Properties of a Combined Bicycle*

and Rider. in ASME Conference Proceedings. 2009: ASME.

[14] Mansfield, N.J et al., *The apparent mass of the seated human exposed to single-axis and multi-axis whole-body vibration.* Journal of Biomechanics, ISSN 0021-9290, 40(11) (2007), 2543-2551.

[15] G. H. M. J. Subashi et al., *Nonlinear subjective and dynamic responses of seated subjects exposed to horizontal whole-body vibration.* Journal of Sound and Vibration, ISSN 0022-460X, 321(1-2) (2009), 416-434.

[16] H.H. Hsu, *The Properties and Human Factor Engineering of the Bicycle with Disk Brake*, in PME Dept. 2001, NTHU: Hsinchu. p. 116.

[17] J.D. Chen, *The Stabilities and Ergonomics of the Bicycle with Disk Brake*, in PME. Dept. 2002, NTHU: Hsinchu. p. 160.

[18] H. Arioui, et al., *Mechatronics, Design, and Modeling of a Motorcycle Riding Simulator*. IEEE/ASME Transactions on Mechatronics(Copyright 2010, The Institution of Engineering and Technology), ISSN 1083-4435, 15(2010), 805-18

[19] Clifford et al., *Measuring Tilt with Low-g Accelerometers.* 2005, Freescale Semiconductor, Inc.

[20] Trimpe, S. et al., *Accelerometer-based tilt estimation of a rigid body with only rotational degrees of freedom.* in Robotics and Automation (ICRA), 2010 IEEE International Conference on. 2010.

[21] Segway Inc., Reference Manual. http://www.segway.com/downloads/pdfs/ReferenceManual.pdf. accessed on 2011-12-26

[22] M.Y. Wang et al., *Static and dynamic anthropometric database of worker population*, Institute of occupational safety and health, Taipei, 1996

[23] J. Wang et al., Anthropometric data book of the Chinese people in Taiwan, ISBN 9789573014904, Hsinchu, Ergonomics Society of Taiwan, 2001

[24] Y.T. Chen, *Control system design and implementation of a pedaled, self-balanced unicycle*, in PME Dept. 2010, NTHU: Hsinchu. p. 91.

Authors

Authors should provide a short biography of authors. Biographies should have a typical length of 5 to 10 lines, in 9,5pt font (\LaTeX: "small"), be limited to main educational background and description of current activities, and preferably be accompanied by a photograph sized 20 by 30 mm. The photograph shall be lined up with the bottom of the text paragraph.

The paper shall be uploaded as a pdf file only, made up to the specifications of this template. In the case special fonts (e.g. symbols) are used, these shall be embedded in the pdf file. The size of the file should not exceed 1,5MB for a total allowed paper length of 12 pages.